THE JOURNAL OF PHYSICAL CHEMISTRY A
A JOURNAL OF THE AMERICAN CHEMICAL SOCIETY

pubs.acs.org/JPCA
Article

Correlated Molecular Orbital Theory Predictions of Hydrogen-Containing Halomethane Thermochemistry: Heats of Formation, C−H Bond Dissociation Energies, and pK_a Values

Thomas Dalton Andress, Cole Seely, Margherita Miele, Laura Castoldi, Vittorio Pace,* and David A. Dixon*

Cite This: J. Phys. Chem. A 2026, 130, 1790−1803
Read Online

ABSTRACT: Heats of formation, bond dissociation energies, proton affinities, gas phase acidities, and pK_a values in water, dimethyl sulfoxide, acetonitrile, and tetrahydrofuran were calculated for all hydrogen-containing halomethanes and methane using composite correlated molecular orbital theory at the G3(MP2) and Feller-Peterson-Dixon (FPD) levels. Notably, the G3(MP2) method was extended to include iodine-containing compounds. The calculated gas phase acidities generally agree with available experimental data within experimental error limits, often within ±4 kJ/mol; however, CH_2F_2 is a significant exception where theory and experiment differ by nearly 40 kJ/mol for the acidity ΔG. Aqueous pK_a values range from 53.6 for CH_3F to 28.0 for CHF_2I. The latter's unexpectedly high acidity results from the CF_2I^- anion resembling a CF_2 carbene interacting with an iodide anion. These computed values rationalize literature base choices for anion generation: trihalomethanes (pK_a 28.0−34.2) are deprotonated by nonorganometallic bases (KOH, DBU, KOtBu), whereas less acidic dihalomethanes (p$K_a \gtrsim 38$), particularly fluorodihalomethanes (pK_a 42−49), require strong metal amides (e.g., LTMP, LDA), with LHMDS proving inadequate. An experimental $CHBrCl_2$ case study corroborates these predictions, showing clean deprotonation with lithium amides compared to diminished efficiency with weaker bases due to competitive hydroxide addition. This work provides the most comprehensive high-accuracy thermochemical data set for the complete set of hydrogen-containing halomethanes.

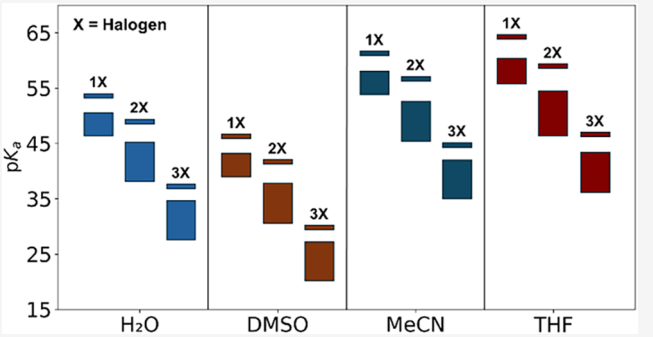

INTRODUCTION

Estimates of the aqueous acidity constants (pK_as) of hydrohalomethanes[1−4] are available for only a few of the 35 compounds even though this class of compounds is one of the most prevalent within organic chemistry with multiple examples likely present in every laboratory. Many of the gas phase C−H bond dissociation energies of the halomethanes are available from Luo's compilation[5] with some species having more reliable values available from the Active Thermochemical Tables (ATcT).[6−8] Nearly half of the hydrogen-containing halomethanes have experimental values for their gas phase acidity[9−15] as summarized in the NIST Webbook.[16] The properties of all halomethane species need to be established as both the Toxic Substances Act and the American Innovation and Manufacturing Act look to limit their availability. Dichloromethane is already being phased out of use by the EPA due to its carcinogenic nature.[17,18]

The inherent acidity of trihalo- and dihalo-methanes makes them excellent precursors for often elusive trihalo- and dihalomethyl- anions.[19,20] These species, referred to as carbenoids, constitute a *unicum* in chemistry, as a consequence of the intrinsic capability to shift from nucleophilic to electrophilic and *vice versa*.[21] This characteristic renders carbenoids key players in C1-insertion processes, as homologations.[22] Besides techniques based on halogen/metal exchange reactions,[23] (poly)halomethyl anions can be conveniently prepared through deprotonation of the corresponding haloforms or methylene halides.[21,24] Obtaining approximate pK_a acidity for these species is critical for selecting the most adequate base enabling the genesis of the desired carbenoid. In fact, both the reactivity regime (nucleophilic or electrophilic) and the chemical integrity can be finely modulated by the countercation.[25,26] For example, lithium carbenoids, generated in the presence of organo-

Received: November 26, 2025
Revised: February 2, 2026
Accepted: February 3, 2026
Published: February 20, 2026

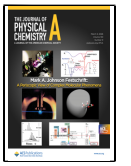

lithiums, predominantly exhibit nucleophilic properties,[21] whereas moving to less positive metals (e.g., Mg, Zn) moves them into the electrophilic regime.[27−29]

Despite their ubiquity, three major gaps undermine the current understanding of halomethane thermodynamics. First, no unified data set exists for all possible halogen combinations, particularly for iodine-containing species due to calculation limitations and the complexities of experimental evaluation such as reactant volatility.[30] Second, the traditional G3(MP2)[31,32] approach does not incorporate iodine which limits the accessibility of low-cost, high-accuracy calculations to nearly half of the hydrohalomethanes. Third, solvent effects in combination with halogen substitution effects remain poorly quantified, as evidenced by the very limited reporting of both experimental and theoretical pK_a values of the hydrohalomethanes. This work seeks to address these gaps by advancing the G3(MP2) model for use in iodomethanes while critically evaluating its accuracy through comparison to available high accuracy experimental data from ATcT as well as the other experimental data.

These knowledge gaps slow progress across multiple domains. Atmospheric modelers lack reliable data for iodine-mediated ozone depletion cycles, materials scientists face uncertainties in designing next-generation halocarbon refrigerants, and synthetic chemists lack information about what is the appropriate choice of a strong base for the generation of carbenoids. Even fundamental theoretical frameworks, such as linear free-energy relationships for halogen substituent effects, remain incomplete without comprehensive thermochemical data spanning the entire halogen series.

Thermochemical parameters such as aqueous pK_a, gas-phase acidity, enthalpy of formation, and bond dissociation energy serve as foundational metrics for predicting chemical reactivity, environmental persistence, and industrial utility. For halomethanes, these properties dictate, in part, their efficacy as refrigerants, solvents, and fire suppressants while simultaneously determining their ozone-depletion potential and global warming contributions. The environmental significance of halomethanes further underscores the urgency of accurate thermochemical characterization. Chlorofluorocarbons (CFCs) and hydrochlorofluorocarbons (HCFCs), once widely used in refrigeration, exemplify how incomplete thermodynamic understanding can lead to unintended environmental consequences.[33] Their atmospheric lifetimes and ozone-depleting potentials are direct functions of bond dissociation energies and reaction enthalpies.[34] These parameters remain minimally studied for mixed-halogen species. Fourth generation refrigerants such as iodine-containing halomethanes present both opportunities as environmentally benign alternatives and challenges due to gaps in their thermochemical profiles.

Experimental determinations of gas-phase acidities have shown intricate substituent effects, where electronegative halogens stabilize conjugate bases through inductive withdrawal while polarizable atoms like iodine enhance acidity via charge delocalization.[16] However, measurements become increasingly challenging for thermally labile or low-volatility species, necessitating reliance on computational predictions as evidenced by the lack of iodine data.

A recent study by Awad[35] employed a combination of experimental data and computational quantum chemistry to evaluate halomethane thermodynamics. Ab initio methods, including Hartree−Fock and composite approaches together with density functional theory (DFT), provided high accuracy predictions of the enthalpies of formation and bond dissociation energies for fluorine-, chlorine-, and bromine-substituted methanes, achieving mean absolute deviations of ≤ 5 kJ/mol from experimental benchmarks although iodine-containing species were not included nor were any energies in solution reported.

COMPUTATIONAL AND EXPERIMENTAL METHODS

Computational Details

All geometries were initially optimized at the density functional theory (DFT) level using the B3LYP[36,37] functional. These optimized geometries were then used as inputs for optimizations at the MP2 level.[38,39] The DFT and MP2 optimizations were both performed with the aug-cc-pVTZ (aT) basis set[40,41] with pseudopotentials (-PP) for Br and I.[42−44] Frequency calculations were performed at both the B3LYP/aT and MP2/aT levels to confirm minima and to obtain zero-point energies (ZPE) and thermal corrections. All optimization and frequency calculations were performed using Gaussian16.[45] The composite correlated molecular orbital theory G3(MP2)[31,32] was then used to predict gas-phase thermochemical values for species not containing iodine as implemented in Gaussian16.

For species containing iodine, we use a modified G3(MP2) approach where the HF optimization and frequency analysis and single point QCISD(T,FC) calculation uses cc-pVDZ-PP basis set for I. The MP2(Full) optimization calculation uses the weighted core basis set cc-pwCVDZ-PP for I, and the single point MP2(FC) calculation uses the weighted core basis set with diffuse functions aug-cc-pwCVTZ-PP for I. All other aspects of the G3(MP2) calculation were kept the same including the high level correction (HLC) values. To the best of our knowledge, this research represents the first instance of an extended G3(MP2) approach with unmodified HLC values.

Using the optimized geometries from the MP2/aT(-PP) level, energies were obtained at the coupled cluster singles and doubles with perturbative triples (CCSD(T))[46] level using the aug-cc-pVnZ (aN, N = T, Q, 5) basis sets.[40,41,47] All CCSD(T) calculations were performed using the MOLPRO software package.[48,49] Open shell calculations were performed with UCCSD(T). Extrapolations to the CBS limit were obtained using eq 1 for two-point extrapolations with n = TQ and Q5 and eq 2 for three-point extrapolations with n = TQ5.[50,51]

$$E_n = E_{CBS} + A(n + 1/2)^{-4} \quad (1)$$

$$E_n = E_{CBS} + A\exp[-(n-1)] + B\exp[-(n-1)^2] \quad (2)$$

Both the scalar relativistic corrections (ΔE_{SR}) and the core-valence corrections (ΔE_{CV}) were obtained at CCSD(T) level. The ΔE_{SR} were calculated at the third order Douglas-Kroll-Hess (DK)[52−55] level with the all-electron basis set aug-cc-pwCVTZ-DK (aT-DK) using eq 3.

$$\Delta E_{SR} = \Delta E_{awCT-DK} - \Delta E_{awCT(-PP,no\ correlation)} \quad (3)$$

The ΔE_{CV} were calculated with aug-cc-pwCVTZ(-PP) (awCT(-PP)) using eq 4.

$$\Delta E_{CV} = \Delta E_{awCT(-PP)} - \Delta E_{awCT(-PP,no\ correlation)} \quad (4)$$

The keyword "CORE,SMALL" in MOLPRO was used when calculating the core-valence correction. C−H frequencies from MP2/aT were scaled by 0.95 to better account for anharmonicity. This scaling value was chosen because it gives the best agreement with spectroscopically derived ZPE values for these species.[56] The scaled ZPE was applied to CCSD(T) energies. The CCSD(T) results were used in the Feller-Peterson-Dixon (FPD) approach[57−60] to total dissociation energies, heats of formation, C−H BDE, gas phase proton affinities, and gas phase acidities. Total dissociation energies (D_0) were calculated according to eq 5.

https://doi.org/10.1021/acs.jpca.5c08066
J. Phys. Chem. A 2026, 130, 1790−1803

Table 1. Gas Phase Heat of Formation at 298 K in kJ/mol

species	B3LYP/aT	G3(MP2)	FPD/Q5	expt. ATcT[6]	ΔE_{expt} (G3(MP2))	ΔE_{expt} (FPD)
CH_4	−75.0	−74.4	−74.1	−74.51 ± 0.043	0.1	0.5
CH_3F	−232.3	−236.0	−234.7	−235.47 ± 0.24	−0.5	0.8
CH_2F_2	−438.8	−451.3	−449.7	−450.93 ± 0.35	−0.4	1.3
CHF_3	−671.4	−696.6	−695.3	−696.23 ± 0.4	−0.4	1.0
CH_3Cl	−66.2	−81.9	−83.5	−82.58 ± 0.17	0.7	−0.9
CH_2Cl_2	−57.1	−95.3	−96.4	−93.7 ± 0.33	−1.6	−2.7
$CHCl_3$	−37.8	−105.8	−103.8	−99.42 ± 0.39	−6.4	−4.4
CH_3Br	−18.7	−37.0	−35.2	−35.85 ± 0.19	−1.2	0.7
CH_2Br_2	43.0	0.6	5.8	5.61 ± 0.59	−5.0	0.2
$CHBr_3$	116.7	43.7	53.9	54.83 ± 0.7	−11.2	−0.9
CH_3I	35.6	16.2	17.6	14.99 ± 0.16	1.2	2.6
CH_2I_2	157.3	109.0	114.9	113.52 ± 0.78	−4.5	1.4
CHI_3	286.0	198.4	212.3	209.3 ± 1.6	−10.9	3.0
CH_2FCl	−242.5	−264.4	−264.8	−263.63 ± 0.85	−0.8	−1.1
CH_2FBr	−189.6	−212.3	−209.5	−211.9 ± 4.9	−0.4	2.4
CH_2FI	−127.8	−150.8	−147.4			
CH_2ClBr	−6.9	−47.1	−45.0	−42.3 ± 1.3	−4.8	−2.7
CH_2ClI	51.2	8.3	11.4			
CH_2BrI	100.6	52.8	61.2			
CHF_2Cl	−450.9	−483.7	−483.1	−481.76 ± 0.99	−1.9	−1.3
CHF_2Br	−394.4	−426.7	−422.9	−424.59 ± 0.47	−2.1	1.7
CHF_2I	−328.5	−360.3	−355.3			
$CHCl_2F$	−239.5	−286.8	−285.8	−283.07 ± 0.9	−3.8	−2.7
$CHCl_2Br$	13.8	−55.7	−50.8	−46.5 ± 1.2	−9.2	−4.3
$CHCl_2I$	73.5	−0.2	7.0			
$CHBr_2F$	−131.3	−179.7	−172.8	−179.3 ± 4.9	−0.4	6.5
$CHBr_2Cl$	65.3	−5.9	1.8	3.2 ± 3.5	−9.1	−1.4
$CHBr_2I$	175.7	93.1	110.0			
CHI_2F	−6.7	−59.5	−50.2			
CHI_2Cl	183.6	104.0	114.6			
CHI_2Br	234.3	149.6	164.9			
CHBrClF	−185.4	−233.2	−229.2	−230.9 ± 4.9	−2.3	1.7
CHIClF	−122.5	−172.2	−166.4			
CHIBrF	−68.8	−121.7	−110.9			
CHIBrCl	124.7	46.6	58.8			

$$D_0 = \sum E_{CBS}\,(\text{atoms}) - E_{CBS}\,(\text{molecule}) + \Delta E_{ZPE} + \Delta E_{SR} + \Delta E_{CV} + \Delta E_{SO} \quad (5)$$

Heats of formation at 298.15 K were calculated by following the procedures outlined by Curtiss et al.[61] using 4.23, 1.05, 4.39, 4.60, 12.26, and 6.61, kJ/mol thermal corrections and 0, −0.33, −1.63, −3.51, −16.69, and −30.33 kJ/mol spin orbit values for H, C, F, Cl, Br, and I, respectively.

Single point solvation calculations with B3LYP and MP2 optimized geometries were performed at the B3LYP/aT and MP2/aT levels using the self-consistent reaction field (SCRF) approach[62] with the conductor like screening model (COSMO)[63,64] and the solvation model based on density (SMD)[65] which includes additional nonelectrostatic terms compared to COSMO.

There are two ways to represent acidity. The first is absolute where the proton contribution is put directly into the calculation (Reaction R1). The other is relative where an experimentally known acid is used in the reaction (Reaction R2).

$$CHX_3 \rightarrow CX_3^- + H^+ \quad (R1)$$

$$CHX_3 + Ac^- \rightarrow CX_3^- + AcH \quad (R2)$$

For gas phase acidity, reaction R1 is used. Solution-phase pK_a values reported in the main text are absolute, obtained from Reaction R1 by combining gas-phase deprotonation free energies with solvation free. For comparison and validation, relative results based on Reaction R2 referenced to benzoic acid are provided in the Supporting Information. Benzoic acid was selected as the reference acid for this study due to the availability of reliable experimental pK_a values across all four solvent systems examined (water, DMSO, MeCN, and THF). Furthermore, the delocalized charge distribution of the benzoate anion is more accurately described by continuum solvation models than that of small, hard oxyanions, minimizing systematic errors associated with the implicit solvation of localized charges. We use pK_a values of 4.25 in water,[66] 21.5 in MeCN,[67] 25.11 in THF,[66] and 11.1 in DMSO[68] for benzoic acid. eq 6 is used to account for the standard state correction which represents the energy change associated with compressing 1 mol of an ideal gas at a presume of 1 atm to a concentration of 1 M.

$$\Delta G^{\circ\rightarrow *} = R \times T \times \ln(24.46) \quad (6)$$

In eq 6, R is the gas constant, T is temperature (298.15 K), and the value 24.46 represents the volume (in liters) occupied by 1 mol of an ideal gas at 298.15 K and 1 atm.

The free energy of solvation is calculated as the difference between the total energy (EE) in solution and the total energy in the gas phase plus the standard state correction as shown in eq 7.

$$\Delta G^*_{solv} = EE^*_{soln} - EE^\circ_{gas} + \Delta G^{\circ\rightarrow *} \quad (7)$$

The absolute solvation free energies of the proton, $\Delta G^*_{solv}(H^+)$, were selected from high-level studies utilizing cluster-continuum methodologies to account for explicit solvent−solute interactions. All

https://doi.org/10.1021/acs.jpca.5c08066
J. Phys. Chem. A 2026, 130, 1790−1803

Table 2. Gas Phase C−H Bond Dissociation Energy (ΔH) at 298 K in kJ/mol

species	B3LYP/aT	G3(MP2)	FPD/Q5	expt. Luo[5]	ΔE_{expt} (G3(MP2))	ΔE_{expt} (FPD)
CH_4	431.7	435.7	436.5	438.99 ± 0.065[a]	−3.3	−2.5
CH_3F	413.1	422.6	421.8	423.8 ± 4.2	−1.2	−2.0
CH_2F_2	413.0	424.6	424.1	431.8 ± 4.2	−7.2	−7.7
CHF_3	432.7	446.2	445.2	446.26 ± 0.6[a]	−0.1	−1.0
CH_3Cl	413.5	415.7	413.6	419.0 ± 2.3	−3.3	−5.4
CH_2Cl_2	391.4	402.2	400.0	402.7 ± 0.94[a]	−0.5	−2.7
$CHCl_3$	384.9	391.7	389.2	392.5 ± 2.5	−0.8	−3.3
CH_3Br	418.4	420.8	420.5	427.2 ± 2.4	−6.4	−6.7
CH_2Br_2	402.2	406.5	407.4	417.1 ± 7.5	−10.6	−9.7
$CHBr_3$	384.1	391.0	392.4	401.7 ± 6.7	−10.7	−9.3
CH_3I	420.5	421.9	421.6	431.0 ± 8.4	−9.1	−9.4
CH_2I_2	400.5	403.7	404.8	431.0 ± 8.4	−27.3	−26.2
CHI_3	376.9	382.5	384.0	423 ± 29	−40.5	−39.0
CH_2FCl	403.1	414.5	413.0	421.7 ± 10.0	−7.2	−8.7
CH_2FBr	411.3	416.3	416.1			
CH_2FI	410.0	414.5	414.5			
CH_2ClBr	400.1	404.4	403.8	406.0 ± 2.4	−1.6	−2.2
CH_2ClI	399.3	402.2	402.5			
CH_2BrI	401.4	404.6	406.1			
CHF_2Cl	418.7	426.0	424.7	421.3 ± 8.4	4.7	3.4
CHF_2Br	413.8	421.9	421.5	415.5 ± 12.6	6.4	6.0
CHF_2I	404.9	413.3	413.1			
$CHCl_2F$	401.5	408.7	406.8	410.9 ± 8.4	−2.2	−4.1
$CHCl_2Br$	384.6	391.4	390.2	387 ± 21	4.4	3.2
$CHCl_2I$	381.1	386.5	386.3			
$CHBr_2F$	397.4	405.4	405.7			
$CHBr_2Cl$	384.3	391.1	391.2	371 ± 21	20.1	20.2
$CHBr_2I$	381.2	387.2	389.2			
CHI_2F	388.2	396.4	396.9			
CHI_2Cl	378.4	384.0	385.0			
CHI_2Br	378.8	384.7	386.9			
CHBrClF	399.4	406.9	406.1	413 ± 21	−6.1	−6.9
CHIClF	393.8	400.9	400.7			
CHIBrF	392.4	400.2	400.7			
CHIBrCl	381.1	386.8	387.6			

[a]Experimental values from ATcT.[6]

values reported herein correspond to a standard state of 1 M in the gas phase transferring to 1 M in solution; therefore, these values already include the state change energy calculated using eq 6.

For water we use an aqueous ΔG^*_{solv} value of − 1097.9 kJ/mol. This is a benchmark value from Zhan and Dixon, derived via a hybrid supermolecule-continuum approach at the CCSD(T)/CBS level which explicitly treats first-shell nonelectrostatic interactions and which has provided good results for previous pK_a studies.[69−71] For DMSO (−1143.5 kJ/mol), the value is taken from Kelly and Truhlar, utilizing cluster-pair approximations validated against independent high-level theoretical estimates.[72] Values for acetonitrile (−1059.4 kJ/mol) and THF (−1075.3 kJ/mol) were taken from recent work utilizing cluster-continuum calculations that account for Boltzmann weighting and entropy of mixing; these values were validated by reproducing the experimental standard hydrogen electrode potentials in their respective solvents.[73]

The solvation contribution ($\Delta\Delta G^*_{solv}$) to the free energy in solution is calculated using eq 8.

$$\Delta\Delta G^*_{solv} = \Delta G^*_{solv}[X_{prod.}] - \Delta G^*_{solv}[X_{react.}] \quad (8)$$

The aqueous free energy in solution (ΔG^*_{aq}) is calculated using eq 9.

$$\Delta G^*_{aq} = \Delta\Delta G^*_{solv} + \Delta G^\circ_{gas} \quad (9)$$

Where ΔG°_{gas} is the gas phase free energy of the reaction at 298.15 K obtained with B3LYP/aT, MP2/aT, G3(MP2), FPD. $\Delta\Delta G_{solv}$ contributions for ΔG_{aq}(G3(MP2)) and ΔG_{aq}(FPD) were calculated using MP2/aT/SCRF. Aqueous pK_a is calculated with ΔG^*_{aq} using eq 10.

$$pK_a = \Delta G^*_{aq}/(R \times T \times \ln(10)) \quad (10)$$

where R is the gas constant and T is temperature. For relative acidities, the experimentally known pK_a is subtracted from the resulting pK_a from eq 10.

A Natural Population Analysis (NPA) based on the Natural Bond Orbital (NBO) method[74,75] using NBO 7[76] was performed on the anions at the MP2/aT level.

Experimental Details

Melting points were determined on a Reichert-Kofler hot-stage microscope and are uncorrected. Mass spectra were obtained on a Shimadzu QP 1000 instrument (EI, 70 eV) and on a Bruker maXis 4G instrument (ESI-TOF, HRMS). ^{1}H, ^{13}C and ^{19} F NMR spectra were recorded on a Bruker Avance III 400 spectrometer (400 MHz for ^{1}H, 100 MHz for ^{13}C, 40 MHz for ^{15}N, 376 MHz for ^{19}F) at 297 K using a, directly detecting broadband observe (BBFO) probe. The center of the solvent signal was used as an internal standard which was related to TMS with δ 7.26 ppm (^{1}H in $CDCl_3$), δ 77.00 ppm (^{13}C in $CDCl_3$). ^{15}N spectra (gsHMBC) were referenced against neat, external nitromethane, ^{19}F NMR spectra by absolute referencing via

https://doi.org/10.1021/acs.jpca.5c08066
J. Phys. Chem. A 2026, 130, 1790−1803

Ξ ratio. Spin−spin coupling constants (J) are given in Hz. In nearly all cases, full and unambiguous assignment of all resonances was performed by combined application of standard NMR techniques, such as APT, HSQC, HMBC, COSY and NOESY experiments.

All of the reactions were carried out under an inert atmosphere of argon. THF was distilled over Na/benzophenone. Chemicals were purchased from Sigma-Aldrich, Acros, Alfa Aesar and TCI Europe. Solutions were evaporated under reduced pressure with a rotary evaporator. TLC was carried out on aluminum sheets precoated with silica gel 60F254 (Merchery-Nagel, Merk); the spots were visualized under UV light (λ = 254 nm).

Specific reaction details and the associated spectra are given in the Supporting Information (SI).

COMPUTATIONAL RESULTS AND DISCUSSION

Gas Phase ΔH_f^0 and BDE

The calculated FPD heats of formation (Table 1) are for in excellent agreement with the experimental values from ATcT[6] with the largest deviation being 6.5 kJ/mol for $CHBr_2F$; note that the experimental value has a larger error bar as well. The largest deviations from experiment at the G3(MP2) level are for the trihalogens $CHBr_3$, CHI_3, $CHCl_2Br$, and $CHBr_2Cl$ which differ by −9 to −11 kJ/mol. Good agreement is found between the G3(MP2) and FPD values with a median absolute difference of 4 kJ/mol highlighting the quality of our modified G3(MP2) approach. CHI_3 is subject to second order spin orbit effects which can be present in closed shell molecules with heavy atoms. For CHI_3, we applied a previously calculated spin orbit correction of −6.3 kJ/mol obtained at the CASPT2/RASSI-SO.[77] An attempt to calculate the spin−orbit correction for CHI_3 using the ADF software[78,79] led to an overestimate of the SO effect. The B3LYP/aT heats of formation are not reliable, and the error tends to grow with increasing number of halogen atoms with a largest error of 77 kJ/mol.

The C−H BDEs are not as well established as the heats of formation with substantially larger error bars. The FPD calculated C−H bond dissociation energies (BDE) are within 4 kJ/mol of the high accuracy experimental ATcT[6] values (Table 2) as are the G3(MP2) values. For the experimental BDEs from Luo,[5] the calculated FPD values are within or just outside the error bars for many of the species. Notable exceptions are CH_2I_2 and CHI_3, which differ from reported values by 26 and 40.5 kJ/mol, respectively. However, we suspect these deviations stem from issues within the experimental compilation rather than computational inaccuracy. The experimental BDE and associated error limits for CH_2I_2 (431.0 ± 8.4 kJ/mol) are numerically identical to those reported for CH_3I in the same reference, strongly suggesting a transcription error in the literature. The experimental value for CHI_3 carries an exceptionally large uncertainty (±29 kJ/mol). In contrast, the modified G3(MP2) method shows excellent internal consistency with our high-level FPD/Q5 benchmarks for these species, deviating by only 1.1 kJ/mol for CH_2I_2 and 1.5 kJ/mol for CHI_3. This suggests the computational results provide a necessary correction to the available experimental data. Another example of an ∼20 kJ/mol difference is $CHBr_2Cl$ but the error bar here is ± 21 kJ/mol. The differences between the calculated values and experiment for CH_2Br_2, $CHBr_3$, and CH_3I are on the order of ±10 kJ/mol, consistent with the larger error bars on the order of ±8 kJ/mol. B3LYP predicts BDEs within about 10 kJ/mol of the FPD values showing a cancellation of error between the parent and the radical.

All of the C−H BDEs except for CHF_3 are less than that for CH_4. The presence of the halogen tends to stabilize the corresponding methyl radical. An increase in the number of halogen substitutions for Cl, Br, and I led to a decrease in the C−H bond energies. This decrease also occurs with increasing halogen size. There is an increase in the C−H bond energy from CH_3F to CHF_3. We examined different correlations of the BDEs with other electronic properties. The C−H BDE is plotted against the isotropic polarizability of the corresponding methyl radical in Figure 1. While the global data set suggests a

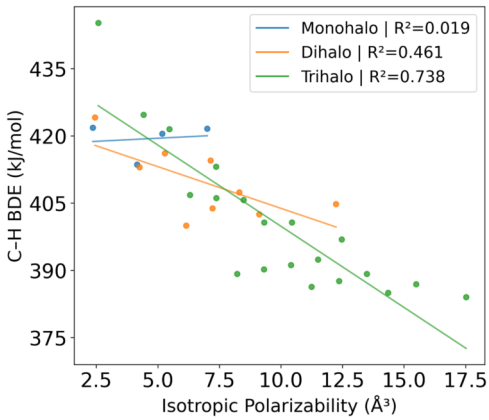

Figure 1. BDE versus isotropic polarizability of the radical resulting from breaking a C−H bond. BDE values from FPD with polarizability from MP2/aT.

general trend (R^2 = 0.736), plotting the data by substitution level reveals distinct electronic behaviors. The monohalomethanes show essentially no correlation (R^2 = 0.019), indicating that polarizability is not a primary determinant of bond strength for these species. However, a correlation emerges for the dihalo species (R^2 = 0.461) and strengthens significantly for the trihalo species (R^2 = 0.738). This progression indicates that the stabilizing effect of radical polarizability is not universal. Instead, it becomes increasingly dominant with higher degrees of halogen substitution.C−H Plots of the BDE vs the spin density on the carbon of the radical product (R^2 = 0.11) or the dipole moment of the radical (R^2 = 0.10) did not yield meaningful correlations.

Gas Phase Electron Affinity of CXYZ•

As the energies for both radical and anion CXYZ species are available, one can readily calculate the electron affinity of the radical (Table 3). The electron affinities are the adiabatic values including ZPE corrections. There is excellent agreement of the FPD values with the experimental values from the NIST Webbook[16] within 0.1 eV for all species except for $CHF_2^•$ which, again, is a species for which the experimental data should be revisited. For $CH_2Br^•$, there are two experimental values[11,80] and there is better agreement between theory and experiment for the larger value.[11] Good agreement, usually within 0.1 eV, is also found between the FPD and G3(MP2) values. A similar trend is found for the electron affinity as with the previous properties where there is an increase in the EA with increasing halogen substitution and an increasing halogen size.

Gas Phase Acidity

The FPD calculated gas phase acidities are in excellent agreement with experimental values[9−16] (Table 4) with most

https://doi.org/10.1021/acs.jpca.5c08066
J. Phys. Chem. A 2026, 130, 1790−1803

Table 3. Electron Affinity (ΔH) at 0 K in eV

species	B3LYP/aT	G3(MP2)	FPD/Q5	expt. NIST[16]	ΔE_{expt} (G3(MP2))	ΔE_{expt} (FPD)
$CH_3^\bullet$	0.11	0.01	0.07	0.080 ± 0.030	−0.07	−0.01
$CH_2F^\bullet$	0.26	0.20	0.19	0.25 ± 0.18	−0.05	−0.06
$CHF_2^\bullet$	0.77	0.73	0.70	1.21 ± 0.16	−0.48	−0.51
$CF_3^\bullet$	1.83	1.77	1.76	1.820 ± 0.050	−0.05	−0.06
$CH_2Cl^\bullet$	0.73	0.75	0.66	0.74 ± 0.16	0.01	−0.08
$CHCl_2^\bullet$	1.48	1.50	1.40	1.472 ± 0.043	0.03	−0.08
$CCl_3^\bullet$	2.15	2.18	2.06	2.160 ± 0.096	0.02	−0.10
$CH_2Br^\bullet$	0.94	0.98	0.91	0.79 ± 0.14	0.19 0.01	0.12 −0.06
				0.97 ± 0.16		
$CHBr_2^\bullet$	1.78	1.82	1.76			
$CBr_3^\bullet$	2.43	2.48	2.41	2.57 ± 0.12	−0.09	−0.16
$CH_2I^\bullet$	1.16	1.18	1.14			
$CHI_2^\bullet$	2.01	2.04	2.01			
$CI_3^\bullet$	2.58	2.64	2.60			
$CHFCl^\bullet$	1.24	1.22	1.13			
$CHFBr^\bullet$	1.46	1.43	1.38			
$CHFI^\bullet$	1.65	1.58	1.58			
$CHClBr^\bullet$	1.64	1.66	1.58			
$CHClI^\bullet$	1.77	1.78	1.73			
$CHBrI^\bullet$	1.90	1.93	1.89			
$CF_2Cl^\bullet$	2.17	2.06	2.02			
$CF_2Br^\bullet$	2.38	2.30	2.28			
$CF_2I^\bullet$	2.55	2.48	2.51			
$CCl_2F^\bullet$	2.21	2.17	2.07			
$CCl_2Br^\bullet$	2.26	2.29	2.18			
$CCl_2I^\bullet$	2.34	2.35	2.26			
$CBr_2F^\bullet$	2.47	2.44	2.38			
$CBr_2Cl^\bullet$	2.35	2.39	2.30			
$CBr_2I^\bullet$	2.49	2.54	2.47			
$CI_2F^\bullet$	2.64	2.59	2.55			
$CI_2Cl^\bullet$	2.47	2.50	2.44			
$CI_2Br^\bullet$	2.54	2.59	2.54			
$CBrClF^\bullet$	2.35	2.30	2.23			
$CIClF^\bullet$	2.46	2.37	2.34			
$CIBrF^\bullet$	2.56	2.51	2.48			
$CIBrCl^\bullet$	2.42	2.45	2.37			

values within 2 kJ/mol of experiment. Species which differ by more are still within the error of the experiment except for CH_2F_2 (ΔE_{expt} = 44.1 kJ/mol) and CHF_2Cl (ΔE_{expt} = −39.6 kJ/mol). However, there are large error bars for these species of ± 15 kJ/mol for CH_2F_2 and ± 30 kJ/mol for CHF_2Cl and we suggest that these experimental values should be revisited. There is good agreement between the G3(MP2) and FPD acidities with a maximum difference of 8.4 kJ/mol between methods and a median absolute difference of 5.7 kJ/mol. B3LYP is able to predict the acidity across the series reasonably well. The gas phase acidity is predicted to decrease with increasing halogen substitution and halogen size.

Figure 2 plots gas phase acidity versus the Mulliken charge on the carbon of the anion with groupings based on the number of halogen substituents and the amount of fluorination. Most R^2 values for these groups are well above 0.9. The $CHXF_2$ trihalo group has a negative slope as a result of the charge now being positive on the carbon. Fluorine substitution is seen to dominate the charge on the carbon as evidenced by the relative slopes of the groups. For example, for the dihalo fluorine group and the dihalo group without F, the slope is significantly steeper for fluorine containing species (m = 658 vs 162). As a specific example, the difference between the charge on the carbon for CH_2F_2 and CH_2FI is Δ = 0.13 versus the difference of Δ = 0.30 for CH_2Cl_2 and CH_2I_2.

Although the correlation for each group is high, the slope of all data points together has an opposite sign as compared to that of the individual groups (except for the $CHXF_2$ trihalo group). This is known as Simpson's reversal[81] and usually signals that there is another variable which may be more appropriate to correlate with/plot against. Figure 3 shows the plot of the gas phase acidity vs the isotropic polarizability of the anion. There is a moderate correlation when the species are grouped by the number of halogen substituents. The points on the left-most of each line are mono-, di-, and trifluoromethanes. Based on these trends, there is a corresponding decrease in the gas phase acidity with increasing polarizability of the anion. This decrease is more pronounced in less substituted halomethanes as evidenced by the change in slope from the mono- to the trihalomethanes. Note that a decrease in the gas phase acidity means a more acidic species.

The gas phase acidity (GA) is composed of the components given in eq 11.

$$GA = BDE(C - H) - EA(CXYZ^\bullet) + IE(H) \quad (11)$$

https://doi.org/10.1021/acs.jpca.5c08066
J. Phys. Chem. A 2026, 130, 1790−1803

Table 4. Gas Phase Acidity (ΔG) at 298 K in kJ/mol

species	B3LYP/aT	G3(MP2)	FPD/Q5	expt.	ΔE_{expt} (G3(MP2))	ΔE_{expt} (FPD)
CH_4	1704.4	1716.8	1710.0	1715 ± 15[9]	1.8	−5.0
CH_3F	1671.5	1685.6	1683.2	1676 ± 17[9]	9.6	7.2
CH_2F_2	1624.5	1639.5	1639.1	1595 ± 15[9]	44.5	44.1
CHF_3	1542.5	1559.8	1557.3	1549 ± 6.3[10]	10.8	8.3
CH_3Cl	1619.0	1624.5	1629.0	1628 ± 13[11]	−3.5	1.0
CH_2Cl_2	1533.9	1541.3	1547.0	1540 ± 8.4[12]	1.3	7.0
$CHCl_3$	1458.2	1465.0	1472.1	1464 ± 8.4[13]	1.0	8.1
CH_3Br	1602.7	1607.0	1611.3	1614 ± 13[11]	−7.0	−2.7
CH_2Br_2	1507.1	1512.6	1519.6	1512 ± 13[12]	0.6	7.6
$CHBr_3$	1427.2	1437.3	1441.1	1431 ± 8.4[12]	6.3	10.1
CH_3I	1584.2	1588.7	1590.3	1587 ± 20[11]	1.7	3.3
CH_2I_2	1483.3	1487.8	1492.4			
CHI_3	1405.2	1409.9	1411.7			
CH_2FCl	1569.1	1577.5	1585.6	1576.1 ± 1.3[14]	1.4	9.5
CH_2FBr	1549.3	1557.3	1565.1			
CH_2FI	1528.7	1540.9	1543.6			
CH_2ClBr	1520.6	1527.0	1532.8	1528 ± 13[12]	−1.0	4.8
CH_2ClI	1506.5	1512.4	1517.4			
CH_2BrI	1496.2	1501.1	1505.4			
CHF_2Cl	1486.4	1506.4	1510.4	1550 ± 30[15]	−43.6	−39.6
CHF_2Br	1460.5	1477.2	1482.2			
CHF_2I	1434.2	1450.9	1449.7			
$CHCl_2F$	1466.3	1481.2	1488.7	1475 ± 8.4[14]	6.2	13.7
$CHCl_2Br$	1444.7	1453.9	1460.9			
$CHCl_2I$	1433.5	1442.0	1449.6			
$CHBr_2F$	1435.8	1449.5	1457.0			
$CHBr_2Cl$	1435.3	1443.8	1450.6			
$CHBr_2I$	1418.8	1425.2	1431.6			
CHI_2F	1410.4	1426.4	1431.7			
CHI_2Cl	1417.3	1424.6	1430.6			
CHI_2Br	1411.6	1417.1	1422.8			
CHBrClF	1449.9	1463.7	1472.1			
CHIClF	1433.4	1450.0	1455.9			
CHIBrF	1421.9	1437.0	1442.6			
CHIBrCl	1425.6	1433.4	1440.2			

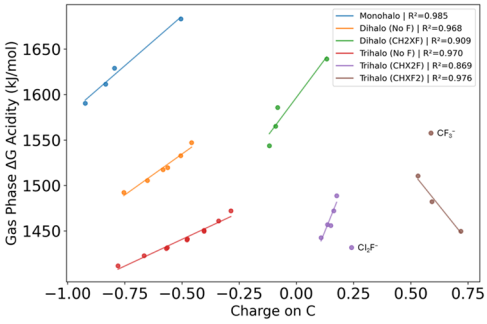

Figure 2. Gas phase acidity versus the NPA charge on the carbon of the resulting anion (MP2/aT) grouped by halogen substitution and fluorination. Methane not shown. CI_2F^- and CF_3^- are not included in their respective groups for the fit and R^2 calculation.

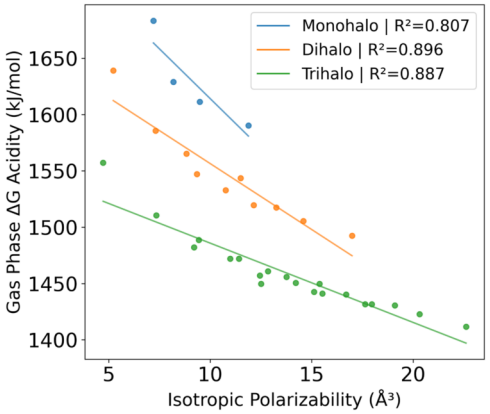

Figure 3. Gas phase acidity versus isotropic polarizability of the resulting anion grouped by the number of halogen substituents. Methane is not shown. Gas phase acidity from FPD with polarizability from MP2/aT.

where EA is the electron affinity of the halomethane radical and IE is the ionization energy of H. Figure 4 shows the correlation between C−H BDE and gas phase acidity grouped by halogen substitution. Similar to the trends observed with polarizability, the correlation between BDE and gas phase acidity is dependent on the degree of substitution. It is nonexistent for monohalomethanes (R^2 = 0.003) but becomes chemically significant for the di- and trihalo series. As halogen substitution increases, so does the sensitivity of the C−H BDE to changes in gas phase acidity as seen in the slopes of each line, a trend similar in magnitude, but opposite in direction, to that seen with gas phase acidity versus polarizability.C−H

https://doi.org/10.1021/acs.jpca.5c08066
J. Phys. Chem. A 2026, 130, 1790−1803

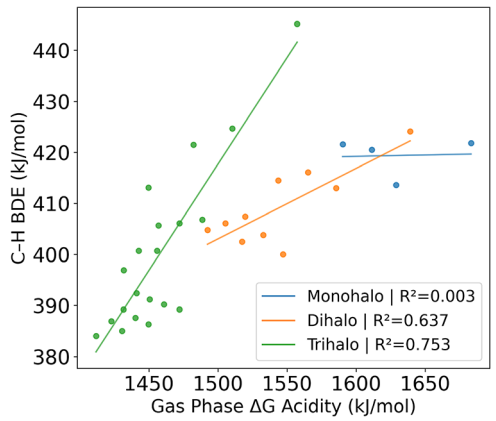

Figure 4. C−H BDE versus gas phase ΔG acidity grouped by the number of halogen substituents. Methane is not shown.

Due to the dependence of gas phase acidity on electron affinity shown in eq 10, we have plotted their relationship in Figure 5. Significant correlation is seen with an R^2 of 0.98. The data shows no evidence of grouping relative to the number of halogen substitutions.

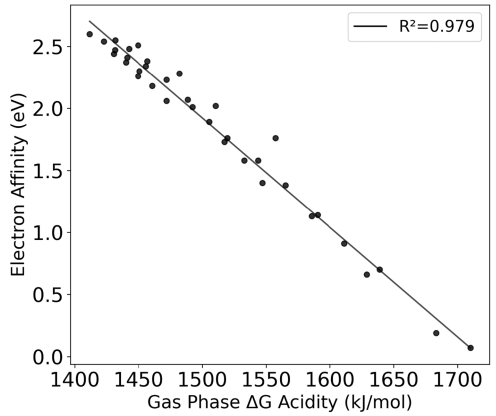

Figure 5. Electron affinity versus gas phase ΔG acidity.

Aqueous Acidity and pK_a

The predicted aqueous acidities and pK_a values calculated using eq 1 are given in Table 5. We predict a general decrease in aqueous acidity (less positive and lower pK_a) with increasing halogen substitution and halogen size. Slight deviations in this trend are observed when using the SMD solvation model. Note that the SMD model includes additional nonelectrostatic contributions which are not present in COSMO. FPD/SMD predicts the highest aqueous acidity values for all except the smallest species.

CHF_2I has a predicted aqueous acidity which is lower than would be expected from simply following the trend of halogen substitution and size with one of the most favorable aqueous acidities across all computational models. This suggests that there are additional factors other than polarizability from the halogen substituents size affecting the aqueous acidity. This point will be elaborated on further in the discussion of our predicted pK_a values. Solvent effects for FPD were obtained by applying the ΔG solvation from MP2/aT geometries as discussed in the computational methods section.

There is very little experimental data on the aqueous pK_as of the hydrogen-containing halomethanes for us to compare our calculated values with (Table 5). The experimental pK_as available from kinetic data shows significant deviation from our calculated values. The Bunnett-Olsen method[82] relies on a linear correlation between the activity coefficient term for the acid of hydrogen halomethane and that of the indicator acid used for comparison. Scharlin[3] notes that the measurements with trichloromethane show large deviations from the ideals of the acidity function concept and notes that the activity coefficient had to be assumed. These same assumptions were made for the determination of the pK_a values of $CHBr_3$, $CHCl_2Br$, and $CHBr_2Cl$; thus these pK_a values may not be correct. Additional experimental problems that could lead to inaccurate determination of pK_a are: (1) Nucleophilic attack of hydroxide which is commonly used. This is particularly true with molecules containing good leaving groups like iodine and bromine. (2) A low degree of ionization due to poor solvation leads to a difficult measurement. (3) There is a modified solvation shell due to the high concentration of base relative to the halomethane.

We predict a general decrease in pK_a (more acidic) with increasing halogen substitution and halogen size. Methane is predicted to have the highest pK_a across all methods. CH_3F is

Table 5. Aqueous Acidity (ΔG_{aq}) in kJ/mol and pK_a Using Gas Phase FPD Values

species	ΔG_{aq}	ΔG_{aq}	pK_a	pK_a	pK_a
	COSMO	SMD	COSMO	SMD	expt
CH_4	319.1	316.1	55.9	55.4	48[1]
CH_3F	305.8	306.2	53.6	53.6	
CH_2F_2	275.8	279.9	48.3	49.0	
CHF_3	206.7	212.9	36.2	37.3	32[2]
CH_3Cl	274.9	282.2	48.2	49.4	
CH_2Cl_2	222.8	235.0	39.0	41.2	
$CHCl_3$	165.7	177.1	29.0	31.0	13.6[3]
CH_3Br	266.4	286.6	46.7	50.2	
CH_2Br_2	208.9	236.4	36.6	41.4	
$CHBr_3$	150.2	175.3	26.3	30.7	11.8[4]
CH_3I	259.2	266.5	45.4	46.7	
CH_2I_2	200.8	219.7	35.2	38.5	
CHI_3	142.8	172.4	25.0	30.2	
CH_2FCl	245.7	255.7	43.1	44.8	
CH_2FBr	235.0	255.2	41.2	44.7	
CH_2FI	227.8	240.5	39.9	42.1	
CH_2ClBr	215.6	235.5	37.8	41.3	
CH_2ClI	211.2	225.9	37.0	39.6	
CH_2BrI	204.8	225.2	35.9	39.5	
CHF_2Cl	182.4	195.3	32.0	34.2	
CHF_2Br	163.6	190.1	28.7	33.3	
CHF_2I	141.2	160.0	24.7	28.0	
$CHCl_2F$	174.2	186.2	30.5	32.6	
$CHCl_2Br$	160.3	176.4	28.1	30.9	12.9[4]
$CHCl_2I$	158.6	175.1	27.8	30.7	
$CHBr_2F$	156.7	181.0	27.5	31.7	
$CHBr_2Cl$	155.2	176.1	27.2	30.8	12.3[4]
$CHBr_2I$	149.1	171.9	26.1	30.1	
CHI_2F	151.5	176.8	26.5	31.0	
CHI_2Cl	151.8	174.6	26.6	30.6	
CHI_2Br	147.4	172.0	25.8	30.1	
CHBrClF	165.1	183.5	28.9	32.1	
CHIClF	160.8	178.7	28.2	31.3	
CHIBrF	153.0	174.8	26.8	30.6	
CHIBrCl	153.5	173.2	26.9	30.3	

https://doi.org/10.1021/acs.jpca.5c08066
J. Phys. Chem. A 2026, 130, 1790−1803

predicted to have the highest pK_a of hydrogen-containing halomethanes across all methods. The third highest pK_as (CH_3X species where X = Cl, Br, I) are ∼5 pK_a units lower. This highlights CH_3F's very low reactivity even among low acidity species.

A moderate correlation is observed between the aqueous pK_a and the solvation contribution of the anion. A stepwise lowering of pK_a is observed with increasing halogen substitution (Figure 6). This is due to the increase in

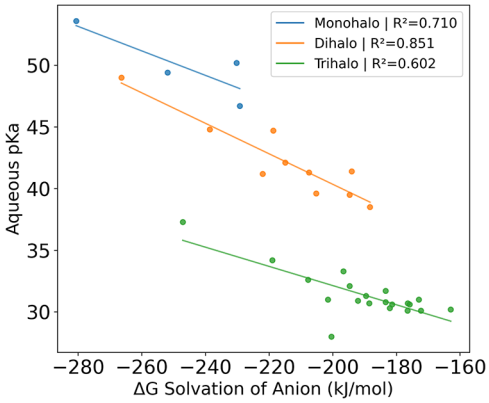

Figure 6. Aqueous pK_a versus MP2/aT/SMD solvation energy of the anion in water. Methane is not shown.

electronegativity and polarizability compared to substituted hydrogen. These increases effectively stabilize the ion in the gas phase resulting in a less negative solvation energy.

The correlation of the aqueous pK_a with the gas phase acidity is given in Figure 7. The good correlation is due to the

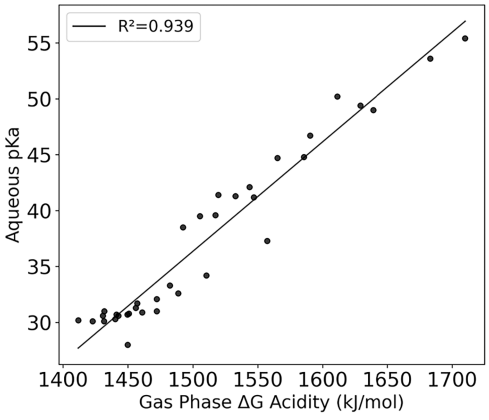

Figure 7. Aqueous pK_a versus gas phase ΔG acidity.

fact that when the gas phase ΔG acidity is higher, i.e., a less stabilized anion in the gas phase, the corresponding ΔG_{solv} of the respective anion will be more negative (more stabilized). Due to the correlation between the pK_a and gas phase acidity, the correlations shown and discussed for gas phase acidity above are applicable to the aqueous pK_a as well.

The most acidic species is predicted to be CHF_2I with a pK_a of 28.0 using FPD/SMD. As noted above, this does not follow the stated trend of a decrease in pK_a with increasing halogen size and substitution. For example, CHI_3, which is expected to have the lowest pK_a based on the trend, is predicted to have a pK_a of 30.2 at the same level. When analyzing the structure of CF_2I^-, it was noticed that the C−I bond length was particularly long. Natural population analysis (NPA) calculations using Gaussian16 were performed on all four CF_2X^- species using MP2/aT with MP2/aT geometries to investigate further. Table 6 summarizes these calculations as well as bond distances associated with these anions. The iodine atom is seen to have a significant portion of the negative charge in CF_2I^-. Table 6 also shows the bond distance change when comparing equivalent radical and anion species. A 0.64 Å increase in C−I bond distance was calculated. These effects are not seen for species like CF_3^-, CF_2Cl^-, or CF_2Br^-. This unique elongation of the C−I bond length in CF_2I^- resembles a CF_2 carbene interacting with an iodide anion and results in the lower-than-expected pK_a.

Nonaqueous pK_a

In addition to aqueous pK_a values, we calculated the pK_a in dimethyl sulfoxide (DMSO), acetonitrile (MeCN), and tetrahydrofuran (THF) (Table 7). A comparison of these values reveals that the solution-phase acidity trends do not follow the solvent dielectric constant (Figure 8).

Instead, the acidity is governed primarily by the solvent's proton affinity (basicity). We observe that the halomethanes are consistently more acidic in DMSO than in water (by approximately 6 pK_a units). This increased acidity arises because DMSO stabilizes the proton more effectively than water (ΔG_{solv} (H^+) in DMSO is more negative by ∼45 kJ/mol), while the solvation free energies of the large, charge-delocalized halomethyl anions remain comparable (average absolute difference ≈ 5.3 kJ/mol) between the two solvents.

In contrast, the pK_a values in MeCN and THF are significantly higher. This is attributed to the weaker proton stabilization in MeCN and the reduced anion solvation in the low-dielectric THF medium (average anion solvation ≈ 22 kJ/mol higher [less negative] in THF compared to other solvents). These results highlight that for carbon acids of this type, specific solvent−proton interactions dominate the thermodynamic profile.

EXPERIMENTAL RESULTS AND DISCUSSION

Generation of (Mixed) Trihalomethyl Anions

There is a good (qualitative) correlation between our calculated pK_a values and the strength of bases employed in literature. The acidifying effect of halogens within the series of haloforms is illustrative. For example, trihalomethyl anions could be successfully generated by the treatment with

Table 6. C−F Bond Lengths (r in Å) and NPA Charges (q in electrons) for CF_2X^- Anions in the Gas Phase

species (CF_2X^-)	q (C)	q (F)	q (X)	r (C−F)	r (C−X)	r (C−X) radical	Δr (anion-neutral)
CF_3^-	0.59	−0.53	−0.53	1.427	1.427	1.317	0.11
CF_2Cl^-	0.53	−0.50	−0.53	1.388	2.057	1.723	0.33
CF_2Br^-	0.59	−0.49	−0.61	1.374	2.297	1.881	0.43
CF_2I^-	0.72	−0.47	−0.78	1.346	2.738	2.101	0.64

https://doi.org/10.1021/acs.jpca.5c08066
J. Phys. Chem. A 2026, 130, 1790−1803

Table 7. pK_a Values in Different Solvents Calculated Using FPD/SMD

species	water	DMSO	MeCN	THF
CH_4	55.4	48.1	63.1	66.7
CH_3F	53.6	46.3	61.3	64.3
CH_2F_2	49.0	41.7	56.6	59.0
CHF_3	37.3	29.9	44.8	46.7
CH_3Cl	49.4	42.1	57.0	59.4
CH_2Cl_2	41.2	33.7	48.6	50.2
$CHCl_3$	31.0	23.6	38.4	39.6
CH_3Br	50.2	42.8	57.7	59.9
CH_2Br_2	41.4	34.0	48.8	49.9
$CHBr_3$	30.7	23.2	38.0	38.7
CH_3I	46.7	39.3	54.2	56.2
CH_2I_2	38.5	31.0	45.8	46.8
CHI_3	30.2	22.6	37.4	37.6
CH_2FCl	44.8	37.4	52.2	54.1
CH_2FBr	44.7	37.3	52.1	53.7
CH_2FI	42.1	34.7	49.5	50.9
CH_2ClBr	41.3	33.8	48.6	50.0
CH_2ClI	39.6	32.1	46.9	48.2
CH_2BrI	39.5	32.0	46.8	47.9
CHF_2Cl	34.2	26.8	41.6	43.0
CHF_2Br	33.3	25.8	40.6	41.6
CHF_2I	28.0	20.6	35.4	36.5
$CHCl_2F$	32.6	25.2	40.0	41.2
$CHCl_2Br$	30.9	23.4	38.2	39.3
$CHCl_2I$	30.7	23.2	38.0	38.8
$CHBr_2F$	31.7	24.2	39.0	39.8
$CHBr_2Cl$	30.8	23.4	38.2	39.0
$CHBr_2I$	30.1	22.6	37.4	37.9
CHI_2F	31.0	25.7	40.4	40.6
CHI_2Cl	30.6	23.1	37.8	38.3
CHI_2Br	30.1	22.6	37.4	37.7
CHBrClF	32.1	24.7	39.5	40.5
CHIClF	31.3	23.8	38.6	39.3
CHIBrF	30.6	23.1	37.9	38.5
CHIBrCl	30.3	22.8	37.6	38.3

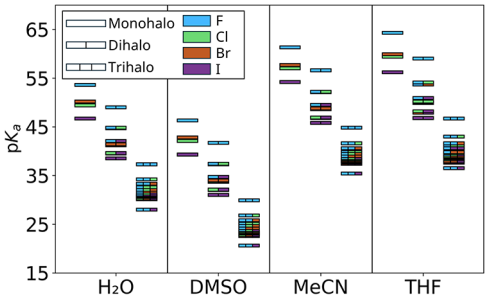

Figure 8. Comparison of pK_a trends between different solvents.

nonorganometallic bases such as KOH[83] or DBU[84] ($CHCl_3$), KOtBu[85] ($CHBr_3$), and KOH[86] (CHI_3). As a consequence, the requirement for stronger bases (e.g., LiHMDS)[87] could be limited to instances in which ensuring proper nucleophilicity of the anion is critical for the transformation or if the recipient electrophile poses chemoselectivity issues.[88] On the other hand, little information (with MeLi, pK_a = 48)[89] is available on the deprotonation of CHF_3,[90] in part due to technical difficulties in the manipulation of this gaseous species and to the extremely high lability of the putative trifluoromethyl anion.[91,92]

Although the series of mixed halo-*difluoro*methanes (CHF_2Cl, CHF_2Br and CHF_2I) have not been used in proton transfer processes, other mixed trihalomethanes have been. For example, Schlosser prepared $LiCCl_2F$[93] starting from $CHCl_2F$ (pK_a = 32.6) and *n*-BuLi (pK_a = 50).[88] However, the need for such a hard base was not found to be mandatory as documented by the successful use of NaOH with this compound[94] or analogues such as $CHBr_2F$[95,96] (pK_a = 31.7), $CHBr_2Cl$[84] (pK_a = 30.8), $CHBr_2I$[97] (pK_a = 30.1), CHI_2Br[96] (pK_a = 30.1), CHI_2F[95] (pK_a = 31.0) and CHI_2Cl[98] (pK_a = 30.6).

Because of the lack of precedents on the application of $CHBrCl_2$ as an anion precursor, we evaluated different bases for generating the corresponding $CBrCl_2^-$ nucleophile. To this end, the facile amidation of (sufficiently electrophilic) isocyanates[99] was selected as the model reaction as shown in Scheme 1. As expected, not only were lithium amides (LDA and LTMP) able to perform the transformation (under Barbier-type conditions),[100] but the weaker DBU (pK_a = 24 in MeCN)[101] and KOH also performed the transformation. Although the efficiency of the process with the latter two was not optimal, presumably also due to the competitive attack of the hydroxide to the isocyanate, their capability to realize the deprotonation was confirmed. We can therefore conclude that (mixed) trihalomethanes featuring a calculated pK_a in the range of 28 to 34 undergo productive deprotonation even with nonorganometallic bases.

Scheme 1. Generation of $CBrCl_2^-$ Anion with Different Bases

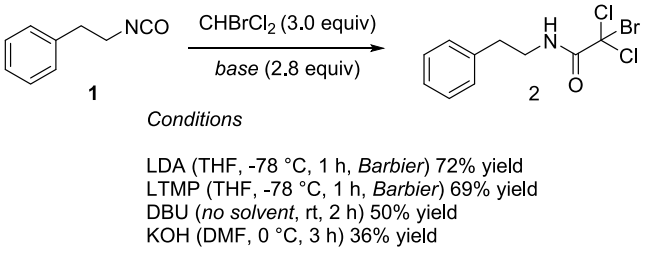

Generation of (Mixed) Dihalomethyl Anions

The significantly lower acidity (higher pK_a) of the dihalomethanes is reflected on the nature of the bases amenable for the effective proton removal. In this sense, metal amides appear to be the reagents of choice regardless of the intercepting electrophile for forming dihalomethyl anions.[102]

(Mixed) dihalomethanes with values of pK_a in the range 38 to 41 (CH_2I_2, CH_2BrI, CH_2ClI, CH_2Cl_2, CH_2Br_2, CH_2ClBr) can be deprotonated not only with harsh basic lithium amides e.g., LTMP,[101,103] LDA,[102] LHMDS[104,105] with pK_as between 30 to 37,[88] but also with less harsh analogues such as NaHMDS[103,104] (CH_2I_2, CH_2ClI, CH_2Br_2 with pK_a = 29.5) or, as shown more recently, with the Knochel-Hauser magnesium amide TMPMgCl-LiCl[106] whose pK_a is unknown.[107]

An interesting effect is observed in the case of two commercially available fluorohalomethyl anion precursors CH_2FI and CH_2FBr.[108] The increased respective pK_a values of 42.1 and 44.7 are diagnostic of requiring lithium amides of compatible strength as only LTMP,[109] LDA[110,111] and LiN(i-Pr)Cy[108] have so far been used successfully. It is worth noting that LHDMS (pK_a = 30)[88] could not be employed for deprotonating these mixed fluorohalomethanes. No data is

https://doi.org/10.1021/acs.jpca.5c08066
J. Phys. Chem. A 2026, 130, 1790−1803

available for CH_2FCl and CH_2F_2 likely due to their gaseous physical state which hampers extensive synthetic applications. In conclusion, as one could expect, the abstraction of protons from dihalomethanes is a more difficult operation requiring strong metal amides bases.

CONCLUSIONS

In this work we have calculated thermochemical data associated with the exhaustive list of hydrogen-containing halomethanes as well as solvent effects on these species. We have shown excellent agreement to the available high accuracy experimental data (within 5 kJ/mol for nearly all gas phase values) with FPD and our modified G3(MP2) which incorporates iodine and extends the ability of low-cost, high-accuracy calculations to the entire set of halomethanes without the need to reparametrize the HLC corrections. For species without experimental data, we report a median absolute difference of < 6 kJ/mol between our FPD and modified G3(MP2) results. Our predicted pK_a values show that the reported experimental values in the literature systematically overestimate the aqueous acidity by ∼ 15 pK_a units for most of these species likely due to assumptions made in their kinetic acidity functions. Proton affinity, electron affinity, and aqueous acidity scale consistently with halogen substitution and size, which are associated with polarizability. However, the trend for C−H bond energy is distinct. The correlation with polarizability is absent in monohalo species but becomes prominent in di- and trihalo species, suggesting that polarizability-driven stabilization requires a threshold of substitution. This indicates that while the thermochemical properties of these species generally correlate with component polarizability, the sensitivity of the C−H bond to these effects is dependent on the degree of substitution.C−H CH_2F_2 differs from our calculated value by nearly 40 kJ/mol for ΔG acidity and a revision of the experimental value is needed. We predict that CH_3F has the least acidic pK_a of the hydrogen-containing halomethanes with a value of 53.6 and CHF_2I has the most acidic pK_a with a value of 28.0 at FPD/SMD primarily due to its anion resembling a CF_2 carbene and an iodine anion. Across water, DMSO, MeCN, and THF, we predict that acidity trends are driven by the solvent's proton affinity (basicity) rather than the dielectric constant, resulting in higher acidities in DMSO and water compared to MeCN and THF. Consistent with the halogen substitution trends, literature base choices for anion generation can now be rationalized. (Mixed) trihalomethanes with calculated pK_a values between 28 and 34 are deprotonated by nonorganometallic bases (e.g., KOH, DBU, KOtBu), whereas the less acidic dihalomethanes (p$K_a \gtrsim 38$) generally require strong metal amides. Fluorodihalomethanes, at the upper end of the pK_a range (pK_a of 42 to 49), require the most basic lithium amides (e.g., LTMP, LDA, LiN(i-Pr)Cy) where LHMDS is inadequate. The $CHBrCl_2$ case study (Scheme 1) further validates these predictions. Lithium amides allow clean deprotonation and interception, whereas weaker bases (DBU, KOH) still generate $CBrCl_2^-$, albeit with reduced efficiency, due to competitive hydroxide addition. The calculated pK_a values thus provide practical guidance for base selection and chemoselectivity for future syntheses.

ASSOCIATED CONTENT

Supporting Information

The Supporting Information is available free of charge at https://pubs.acs.org/doi/10.1021/acs.jpca.5c08066.

Total dissociation energies, thermochemical components for FPD, proton affinities, solvation energies, absolute pK_as, total energies in a.u., and optimized coordinates in Å; additional experimental details (PDF)

AUTHOR INFORMATION

Corresponding Authors

Vittorio Pace − *University of Rome "La Sapienza", Department of Chemistry, Rome 00185, Italy; University of Vienna, Department of Pharmaceutical Sciences, Division of Pharmaceutical Chemistry, Vienna 1090, Austria;* orcid.org/0000-0003-3037-5930; Email: vittorio.pace@uniroma1.it

David A. Dixon − *Department of Chemistry and Biochemistry, Shelby Hall, The University of Alabama, Tuscaloosa, Alabama 35487, United States;* orcid.org/0000-0002-9492-0056; Email: dadixon@ua.edu

Authors

Thomas Dalton Andress − *Department of Chemistry and Biochemistry, Shelby Hall, The University of Alabama, Tuscaloosa, Alabama 35487, United States*

Cole Seely − *Department of Chemistry and Biochemistry, Shelby Hall, The University of Alabama, Tuscaloosa, Alabama 35487, United States*

Margherita Miele − *University of Turin, Department of Chemistry, Turin 10125, Italy*

Laura Castoldi − *University of Milan, Department of Pharmaceutical Sciences, General and Organic Chemistry Section "A. Marchesini", Milan 20133, Italy*

Complete contact information is available at: https://pubs.acs.org/10.1021/acs.jpca.5c08066

Notes

The authors declare no competing financial interest.

ACKNOWLEDGMENTS

The work was supported by UNCAGE-ME, an Energy Frontier Research Center funded by the United States Department of Energy, Office of Science, Basic Energy Sciences under Award DE-SC0012577. The EFRC is led by the Georgia Institute of Technology. DAD also thanks the Robert Ramsay Chair and Endowed Shelby Distinguished Professor Funds of The University of Alabama for support.

DEDICATION

This work is dedicated to the memory of Professor David A. Dixon, whose untimely passing during the completion of this publication represents an immeasurable loss to the field of computational chemistry and to all who had the privilege of knowing him. Professor Dixon was a pioneering scientist whose contributions to theoretical and computational chemistry have shaped our understanding of chemical systems. Though he is no longer here to see its completion, his influence remains in every page of this publication. It is our hope that this work reflects the standards he set and honors the

https://doi.org/10.1021/acs.jpca.5c08066
J. Phys. Chem. A 2026, 130, 1790−1803

legacy of a remarkable scientist, mentor, and teacher. D.A.D. (1949−2026)

REFERENCES

(1) Smith, M. B.; March, J. *March's Advanced Organic Chemistry*; John Wiley & Sons, Inc: Hoboken, NJ, 2007.

(2) Reich, H. J.Bordwell pK_a Table in the Hans Reich's Collection. https://organicchemistrydata.org/hansreich/resources/pka/. (accessed January 1, 2025).

(3) Scharlin, P.; Døssing, A.; Nielsen, K. M.; et al. Application of Acidity Function Method to the Determination of pK_a Values of Trihalomethanes. I. Trichloromethane. *Acta Chem. Scand. A* **1986**, *40a*, 207−209.

(4) Scharlin, P. Evaluation of pK_a Values for Bromodichloromethane, Chlorodibromomethane, and Tribromomethane from Kinetic Acidites. *Acta Chem. Scand. A* **1987**, *41*, 480−483.

(5) Luo, Y. R. *Comprehensive Handbook of Chemical Bond Energies*; CRC Press: Boca Raton, FL, 2007.

(6) Ruscic, B.; Bross, D. H. Active Thermochemical Tables (ATcT) Values Version 1.220 of the Thermochemical Network; ANL 2025. https://atct.anl.gov/Thermochemical%20Data/version%201.220/index.php. (accessed March 1, 2025).

(7) Ruscic, B.; Pinzon, R. E.; Morton, M. L.; von Laszewski, G.; Bittner, S.; Nijsure, S. G.; Amin, K. A.; Minkoff, M.; Wagner, A. F. Introduction to Active Thermochemical Tables: Several "Key" Enthalpies of Formation Revisited. *J. Phys. Chem. A* **2004**, *108*, 9979−9997.

(8) Ruscic, B.; Bross, D. H.Thermochemistry. In *Computer Aided Chemical Engineering*; Elsevier, 2019; Vol. *45*, pp 3−114.

(9) Graul, S. T.; Squires, R. R. Gas-Phase Acidities Derived from Threshold Energies for Activated Reactions. *J. Am. Chem. Soc.* **1990**, *112*, 2517−2529.

(10) Deyerl, H. J.; Alconcel, L. S.; Continetti, R. E. Photodetachment Imaging Studies of the Electron Affinity of CF_3. *J. Phys. Chem. A* **2001**, *105*, 552−557.

(11) Ingemann, S.; Nibbering, N. M. M. Gas-Phase Acidity of CH_3X [X = $P(CH_3)_2$, SCH_3, F, Cl, Br, I] Compounds. *J. Chem. Soc. Perkin Trans. 2* **1985**, No. 6, 837−840.

(12) Born, M.; Ingemann, S.; Nibbering, N. M. M. Thermochemical Properties of Halogen-Substituted Methanes, Methyl Radicals, and Carbenes in the Gas Phase. *Int. J. Mass Spectrom.* **2000**, *194*, 103−113.

(13) Paulino, J. A.; Squires, R. R. Carbene Thermochemistry from Collision-Induced Dissociation Threshold Energy Measurements - The Heats of Formation of X^1A_1 CF_2 and X^1A_1 CCl_2. *J. Am. Chem. Soc.* **1991**, *113*, 5573−5580.

(14) Poutsma, J. C.; Paulino, J. A.; Squires, R. R. Absolute Heats of Formation of CHCl, CHF, and CClF. A Gas-Phase Experimental and G2 Theoretical Study. *J. Phys. Chem. A* **1997**, *101*, 5327−5336.

(15) Dispert, H.; Lacmann, K. Negative Ion Formation in Collisions Between Potassium and Fluoro- and Chloromethanes: Electron Affinities and Bond Dissociation Energies. *Int. J. Mass Spectrom. Ion Phys.* **1978**, *28*, 49−67.

(16) NIST Chemistry WebBook.. NIST Standard Reference Database Number 69, Negative Ion Energetics Data Bartmess, J. E., Ed.; NIST, 2023.

(17) U.S. Environmental Protection Agency.. *A Guide to Complying with the 2024 Methylene Chloride Regulation Under the Toxic Substances Control Act (TSCA); EPA Document #740S2401* U.S. Environmental Protection Agency: Washington, DC; 20241-42.

(18) U.S. Environmental Protection Agency.. *Final Risk Management Rule for Methylene Chloride under TSCA; EPA Document #740F24014* U.S. Environmental Protection Agency: Washington, DC; 20241-2.

(19) Pace, V.; Holzer, W.; De Kimpe, N. Lithium Halomethylcarbenoids: Preparation and Use in the Homologation of Carbon Electrophiles. *Chem. Rec.* **2016**, *16*, 2061−2076.

(20) Ielo, L.; Pace, V. *Science of Synthesis*, 1st ed.; Georg Thieme Verlag KG: Stuttgart, 2025; Vol. *2025/2*, pp 39−91.

(21) Castoldi, L.; Monticelli, S.; Senatore, R.; Ielo, L.; Pace, V. Homologation chemistry with nucleophilic [small alpha]-substituted organometallic reagents: chemocontrol, new concepts and (solved) challenges. *Chem. Commun.* **2018**, *54*, 6692−6704.

(22) Ielo, L.; Miele, M.; Pillari, V.; Castoldi, L.; Pace, V. Lithium Carbenoids in Homologation Chemistry. In *Homologation Reactions: Reagents, Applications, and Mechanisms*; Pace, V., Ed.; Wiley-VCH: Weinheim, Germany, 2023; pp 79−142.

(23) Braun, M. Lithium Carbenoids. In *PATAI'S Chemistry of Functional Groups*; John Wiley & Sons, Ltd, 2009.

(24) Castoldi, L.; Holzer, W.; Langer, T.; Pace, V. Evidence and isolation of tetrahedral intermediates formed upon the addition of lithium carbenoids to Weinreb amides and N-acylpyrroles. *Chem. Commun.* **2017**, *53*, 9498−9501.

(25) Capriati, V.; Florio, S. Anatomy of Long-Lasting Love Affairs with Lithium Carbenoids: Past and Present Status and Future Prospects. *Chem. - Eur. J.* **2010**, *16*, 4152−4162.

(26) Gessner, V. H. Stability and reactivity control of carbenoids: recent advances and perspectives. *Chem. Commun.* **2016**, *52*, 12011−12023.

(27) Satoh, T. Recent advances in the chemistry of magnesium carbenoids. *Chem. Soc. Rev.* **2007**, *36*, 1561−1572.

(28) Satoh, T. Recent Advances in the Chemistry and Synthetic Uses of Magnesium Carbenoids. *Heterocycles* **2012**, *85*, 1−33.

(29) Pasco, M.; Gilboa, N.; Mejuch, T.; Marek, I. The Renaissance of Zinc Carbenoid in Stereoselective Synthesis in Acyclic Systems. *Organometallics* **2013**, *32*, 942−950.

(30) Grubel, K.; Rosenthal, W. S.; Autrey, T.; Henson, N. J.; Koh, K.; Flowers, S.; Blake, T. A. An Experimental, Computational, and Uncertainty Analysis Study of the Rates of Iodoalkane Trapping by DABCO in Solution Phase Organic Media. *Phys. Chem. Chem. Phys.* **2023**, *25*, 6914−6926.

(31) Curtiss, L. A.; Raghavachari, K.; Pople, J. A. Gaussian-3 Theory Using Reduced Møller-Plesset Order. *J. Chem. Phys.* **1999**, *110*, 4703−4709.

(32) Curtiss, L. A.; Redfern, P. C.; Rassolov, V.; Kedziora, G.; Pople, J. A. Extension of Gaussian-3 Theory to Molecules Containing Third-Row Atoms K, Ca, Ga−Kr. *J. Chem. Phys.* **2001**, *114*, 9287−9295.

(33) Wallington, T. J.; Schneider, W. F.; Worsnop, D. R.; Neilsen, O. J.; Sehested, J.; DeBruyn, W. J.; Shorter, J. A. The Environmental Impact of CFC Replacements−HFCs and HCFCs. *Environ. Sci. Technol.* **1994**, *28*, 320A−326A.

(34) Nimitz, J. S.; Skaggs, S. R. Estimating Tropospheric Lifetimes and Ozone-Depletion Potentials of One- and Two-Carbon Hydrofluorocarbons and Hydrochlorofluorocarbons. *Environ. Sci. Technol.* **1992**, *26*, 739−744.

(35) Awad, I. E. Investigation of Thermodynamic Properties of Halomethanes Using High-Level Ab Initio Computations: Evaluation of Enthalpy of Formation and Carbon-Halogen Bond Dissociation Energies. *Turkish Comp. Theo. Chem.* **2025**, *9*, 121−134.

(36) Becke, A. D. Density-Functional Thermochemistry. III. The Role of Exact Exchange. *J. Chem. Phys.* **1993**, *98*, 5648−5652.

(37) Lee, C.; Yang, W.; Parr, R. G. Accurate and Simple Analytic Representation of the Electron Gas Correlation Energy. *Phys. Rev. B* **1988**, *37*, 785−789.

(38) Møller, C.; Plesset, M. S. Note on an Approximation Treatment for Many-Electron Systems. *Phys. Rev.* **1934**, *46*, 618−622.

(39) Pople, J. A.; Binkley, J. S.; Seeger, R. Theoretical Models Incorporating Electron Correlation. *Int. J. Quantum Chem.* **2009**, *10*, 1−19.

(40) Woon, D. E.; Dunning, T. H., Jr. Gaussian Basis Sets for Use in Correlated Molecular Calculations. V. Core-Valence Basis Sets for Boron through Neon. *J. Chem. Phys.* **1995**, *103*, 4572−4585.

(41) Peterson, K. A.; Dunning, T. H. Accurate Correlation Consistent Basis Sets for Molecular Core-Valence Correlation Effects: The Second Row Atoms Al−Ar, and the First Row Atoms B−Ne Revisited. *J. Chem. Phys.* **2002**, *117*, 10548−10560.

https://doi.org/10.1021/acs.jpca.5c08066
J. Phys. Chem. A 2026, 130, 1790−1803

(42) Kendall, R. A.; Dunning, T. H., Jr.; Harrison, R. J. Electron Affinities of the First Row Atoms Revisited. Systematic Basis Sets and Wave. *Funct. J. Chem. Phys.* **1992**, *96*, 6796−6806.
(43) Peterson, K. A.; Yousaf, K. E. Molecular Core-Valence Correlation Effects Involving the Post-d Elements Ga-Rn: Benchmarks and New Pseudopotential-Based Correlation Consistent Basis Sets. *J. Chem. Phys.* **2010**, *133*, No. 174116.
(44) Peterson, K. A.; Shepler, B. C.; Figgen, D.; Stoll, H. On the Spectroscopic and Thermochemical Properties of ClO, BrO, IO, and their Anions. *J. Phys. Chem. A* **2006**, *110*, 13877−13883.
(45) Frisch, M. J.; Trucks, G. W.; Schlegel, H. B.; Scuseria, G. E.; Robb, M. A.; Cheeseman, J. R.; Scalmani, G.; Barone, V.; Petersson, G. A.; Nakatsuji, H.; Li, X.; Caricato, M.; Marenich, A. V.; Bloino, J.; Janesko, B. G.; Gomperts, R.; Mennucci, B.; Hratchian, H. P.; Ortiz, J. V.; Izmaylov, A. F.; Sonnenberg, J. L.; Williams-Young, D.; Ding, F.; Lipparini, F.; Egidi, F.; Goings, J.; Peng, B.; Petrone, A.; Henderson, T.; Ranasinghe, D.; Zakrzewski, V. G.; Gao, J.; Rega, N.; Zheng, G.; Liang, W.; Hada, M.; Ehara, M.; Toyota, K.; Fukuda, R.; Hasegawa, J.; Ishida, M.; Nakajima, T.; Honda, Y.; Kitao, O.; Nakai, H.; Vreven, T.; Throssell, K.; Montgomery, J. A., Jr.; Peralta, J. E.; Ogliaro, F.; Bearpark, M. J.; Heyd, J. J.; Brothers, E. N.; Kudin, K. N.; Staroverov, V. N.; Keith, T. A.; Kobayashi, R.; Normand, J.; Raghavachari, K.; Rendell, A. P.; Burant, J. C.; Iyengar, S. S.; Tomasi, J.; Cossi, M.; Millam, J. M.; Klene, M.; Adamo, C.; Cammi, R.; Ochterski, J. W.; Martin, R. L.; Morokuma, K.; Farkas, O.; Foresman, J. B.; Fox, D. J. *Gaussian 16, Revision A.03*; Gaussian, Inc.: Wallingford CT, 2016.
(46) Tew, D. P.; Klopper, W.; Neiss, C.; Hättig, C. Quintuple-ζ Quality Coupled-Cluster Correlation Energies with Triple- ζ Basis Sets. *Phys. Chem. Chem. Phys.* **2007**, *9*, 1921−1930.
(47) de Jong, W. A.; Harrison, R. J.; Dixon, D. A. Parallel Douglas-Kroll Energy and Gradients in NWChem: Estimating Scalar Relativistic Effects Using Douglas-Kroll Contracted Basis Sets. *J. Chem. Phys.* **2001**, *114*, 48−53.
(48) Werner, H.-J.; Knowles, P. J.; Knizia, G.; Manby, F. R.; Schütz, M.; Celani, P.; Györffy, W.; Kats, D.; Korona, T.; Lindh, R.; Mitrushenkov, A.; Rauhut, G.; Shamasundar, K. R.; Adler, T. B.; Amos, R. D.; Bennie, S. J.; Bernhardsson, A.; Berning, A.; Cooper, D. L.; Deegan, M. J. O.; Dobbyn, A. J.; Eckert, F.; Goll, E.; Hampel, C.; Hesselmann, A.; Hetzer, G.; Hrenar, T.; Jansen, G.; Köppl, C.; Lee, S. J. R.; Liu, Y.; Lloyd, A. W.; Ma, Q.; Mata, R. A.; May, A. J.; McNicholas, S. J.; Meyer, W.; Miller, T. F., III; Mura, M. E.; Nicklass, A.; O'Neill, D. P.; Palmieri, P.; Peng, D.; Petrenko, T.; Pflüger, K.; Pitzer, R.; Reiher, M.; Shiozaki, T.; Stoll, H.; Stone, A. J.; Tarroni, R.; Thorsteinsson, T.; Wang, M.; Welborn, M. *MOLPRO, Version 2020.1, A Package Of Ab Initio Programs*, MOLPRO https://www.molpro.net. (accessed December 1, 2021).
(49) Werner, H.-J.; Knowles, P. J.; Manby, F. R.; Black, J. A.; Doll, K.; Heßelmann, A.; Kats, D.; Köhn, A.; Korona, T.; Kreplin, D. A.; Ma, Q.; Miller, T. F., III; Mitrushchenkov, A.; Peterson, K. A.; Polyak, I.; Rauhut, G.; Sibaev, M. The Molpro Quantum Chemistry Package. *J. Chem. Phys.* **2020**, *152*, No. 144107.
(50) Martin, J. M. L. *Ab Initio* Total Atomization Energies of Small Molecules - Towards the Basis Set Limit. *Chem. Phys. Lett.* **1996**, *259*, 669−678.
(51) Feller, D.; Peterson, K. A.; Hill, J. G. On the Effectiveness of CCSD(T) Complete Basis set Extrapolations for Atomization Energies. *J. Chem. Phys.* **2011**, *135*, No. 044102.
(52) Bross, D. H.; Peterson, K. A. Correlation Consistent, Douglas-Kroll-Hess Relativistic Basis Sets for the 5p and 6p Elements. *Theor. Chem. Acc.* **2014**, *133*, No. 1434.
(53) Douglas, M.; Kroll, N. M. Quantum Electrodynamical Corrections to the Fine Structure of Helium. *Ann. Phys.* **1974**, *82*, 89−155.
(54) Hess, B. A. Applicability of the No-Pair Equation with Free-Particle Projection Operators to Atomic and Molecular Structure Calculations. *Phys. Rev. A* **1985**, *32*, 756−763.
(55) Hess, B. A. Relativistic Electronic-Structure Calculations Employing a Two-Component No-Pair Formalism with External-Field Projection Operators. *Phys. Rev. A* **1986**, *33*, 3742−3748.
(56) Shimanouchi, T. *Tables of Molecular Vibrational Frequencies; NSRDS-NBS 39* National Bureau of Standards: Washington, DC; 1972.
(57) Dixon, D. A.; Feller, D.; Peterson, K. A. A Practical Guide to Reliable First Principles Computational Thermochemistry Predictions Across the Periodic Table. In *Annual Reports in Computational Chemistry*; Ralph, A. W., Ed.; Elsevier, 2012; Vol. *8*, pp 1−28.
(58) Peterson, K. A.; Feller, D.; Dixon, D. A. Chemical Accuracy in *ab Initio* Thermochemistry and Spectroscopy: Current Strategies and Future Challenges. *Theor. Chem. Acc.* **2012**, *131*, No. 1079.
(59) Feller, D.; Peterson, K. A.; Dixon, D. A. Further Benchmarks of a Composite, Convergent, Statistically Calibrated Coupled Cluster Based Approach for Thermochemical and Spectroscopic Studies. *Mol. Phys.* **2012**, *110*, 2381−2399.
(60) Feller, D.; Peterson, K. A.; Dixon, D. A. The Impact of Larger Basis Sets and Explicitly Correlated Coupled Cluster Theory on the Feller-Peterson-Dixon Composite Method. In *Annual Reports in Computational Chemistry*; Dixon, D. A., Ed.; Elsevier: Amsterdam, 2016; Vol. *12*, pp 47−78.
(61) Curtiss, L. A.; Raghavachari, K.; Redfern, P. C.; Pople, J. A. Assessment of Gaussian-2 and Density Functional Theories for the Computation of Enthalpies of Formation. *J. Chem. Phys.* **1997**, *106*, 1063−1079.
(62) Tomasi, J.; Mennucci, B.; Cammi, R. Quantum Mechanical Continuum Solvation Models. *Chem. Rev.* **2005**, *105*, 2999−3093.
(63) Klamt, A. *COSMO RS, Quantum Chemistry to Fluid Phase Thermodynamics and Drug Design*; Elsevier: Amsterdam, 2005.
(64) Klamt, A.; Schuurmann, G. COSMO: A New Approach to Dielectric Screening in Solvents with Explicit Expressions for the Screening Energy and Its Gradient. *J. Chem. Soc., Perkin Trans. 2,* **1993**, *2*, 799−805.
(65) Marenich, A. V.; Cramer, C. J.; Truhlar, D. G. Universal Solvation Model Based on Solute Electron Density and a Continuum Model of the Solvent Defined by the Bulk Dielectric Constant and Atomic Surface Tensions. *J. Phys. Chem. B* **2009**, *113*, 6378−6396.
(66) Kütt, A.; Selberg, S.; Kaljurand, I.; Tshepelevitsh, S.; Heering, A.; Darnell, A.; Kaupmees, K.; Piirsalu, M.; Leito, I. pK_a Values in Organic Chemistry − Making Maximum use of the Available Data. *Tetrahedron Lett.* **2018**, *59*, 3738−3748.
(67) Kütt, A.; Tshepelevitsh, S.; Saame, J.; Lõkov, M.; Kaljurand, I.; Selberg, S.; Leito, I. Strengths of Acids in Acetonitrile. *Eur. J. Org. Chem.* **2021**, *2021*, 1407−1419.
(68) Reich, H. Equilibrium pKa Table (DMSO Solvent and Reference)ACS Division of Organic Chemistry; ACS Division of Organic Chemistry, 2024. https://organicchemistrydata.org/hansreich/resources/pka/pka_data/pka-compilation-reich-bordwell.pdf. (accessed January 1, 2025).
(69) Zhan, C. G.; Dixon, D. A. Absolute Hydration Free Energy of the Proton from First-Principles Electronic Structure Calculations. *J. Phys. Chem. A* **2001**, *105*, 11534−11540.
(70) Feng, R.; Vasiliu, M.; Peterson, K. A.; Dixon, D. A. Acidity of M(VI)O_2(OH)$_2$ for M = Group 6, 16, and U as Central Atoms. *J. Phys. Chem. A* **2017**, *121*, 1041−1050.
(71) Lee, Z. R.; Quinn, L. J.; Jones, C. W.; Hayes, S. E.; Dixon, D. A. Predicting the Mechanism and Products of CO_2 Capture by Amines in the Presence of H_2O. *J. Phys. Chem. A* **2021**, *125*, 9802−9818.
(72) Kelly, C. P.; Cramer, C. J.; Truhlar, D. G. Single-Ion Solvation Free Energies and the Normal Hydrogen Electrode Potential in Methanol, Acetonitrile, and Dimethyl Sulfoxide. *J. Phys. Chem. B* **2007**, *111*, 408−422.
(73) Duda, D. P.; Sprouse, S.; Hu, Y.; Wiedner, E. S.; Dixon, D. A. Redox Potential for Hydrogen Species in Acetonitrile and Tetrahydrofuran *J. Phys. Chem. A.*
(74) Weinhold, F.; Landis, C. R. *Valency and Bonding: A Natural Bond Orbital Donor-Acceptor Perspective*, University Press: Cambridge, U.K., 2005.
(75) Reed, A. E.; Curtiss, L. A.; Weinhold, F. Intermolecular Interactions from a Natural Bond Orbital, Donor-Acceptor Viewpoint. *Chem. Rev.* **1988**, *88*, 899−926.

https://doi.org/10.1021/acs.jpca.5c08066
J. Phys. Chem. A 2026, 130, 1790−1803

(76) Glendening, E. D.; Badenhoop, J. K.; Reed, A. E.; Carpenter, J. E.; Bohmann, J. A.; Morales, C. M.; Karafiloglou, P.; Landis, C. R.; Weinhold, F. *Natural Bond Order 7.0*; Theoretical Chemistry Institute, University of Wisconsin: Madison, WI, 2018.
(77) Sudolská, M.; Louis, F.; Černušak, I. Reactivity of CHI3 with OH Radicals: X-Abstraction Reaction Pathways (X = H, I), Atmospheric Chemistry, and Nuclear Safety. *J. Phys. Chem. A* **2014**, *118*, 9512−9520.
(78) *ADF Release, ADF Users Guide, SCM. Theoretical Chemistry*; Vrije Universiteit: Amsterdam, 2016 https://www.scm.com/doc/ADF/downloads/ADF.pdf.
(79) Te Velde, G.; Bickelhaupt, F. M.; van Gisbergen, S. J. A.; Fonseca Guerra, C.; Baerends, E. J.; Snijders, J. G.; Ziegler, T. Chemistry with ADF. *J. Comput. Chem.* **2001**, *22*, 931−967.
(80) Hierl, P. M.; Henchman, M. J.; Paulson, J. F. Threshold Energies for the Reactions HO^- + MeX - MeOH + X^- measured by Tandem Mass Spectrometry: Acidities of MeCl and MeBr. *Int. J. Mass Spectrom. Ion Proc.* **1992**, *117*, 475−485.
(81) Simpson, E. H. The Interpretation of Interaction in Contingency Tables. *J. R. Stat. Soc. Ser. B* **1951**, *13*, 238−241.
(82) Bunnett, J. F.; Olsen, F. P. Linear Free Energy Relationships Concerning Reaction Rates in Moderately Concentrated Mineral Acids. *Can. J. Chem.* **1966**, *44*, 1917−1931.
(83) Wyvratt, J. M.; Hazen, G. G.; Weinstock, L. M. A convenient, general synthesis of. alpha.-trichloromethyl carbinols. *J. Org. Chem.* **1987**, *52*, 944−945.
(84) Aggarwal, V. K.; Mereu, A. Amidine-Promoted Addition of Chloroform to Carbonyl Compounds. *J. Org. Chem.* **2000**, *65*, 7211−7212.
(85) Sedenkova, K. N.; Averina, E. B.; Grishin, Y. K.; Rybakov, V. B.; Kuznetzova, T. S.; Zefirov, N. S. Cationic Carbenoid Rearrangement of 2-Phenyl Substituted gem-Dihalogenospiropentanes. *Eur. J. Org. Chem.* **2010**, *2010*, 4145−4150.
(86) Duchardt, K. H.; Kröhnke, F. Trihalogenmethyl)-dihydropyridine. *Chem. Ber.* **1977**, *110*, 2669−2679.
(87) Charreau, P.; Julia, M.; Verpeaux, J. N. Nucleophilic and electrophilic properties of diiodomethyl lithium and sodium. Preparation of 1,1-diiodoalkanes and 1-iodoalkenes. *Bull. Chem. Soc. Fr.* **1990**, *127*, 275−282.
(88) Brantley, S. E.; Molinski, T. F. Synthetic Studies of Trichloroleucine Marine Natural Products. Michael Addition of LiCCl3 to N-Crotonylcamphor Sultam. *Org. Lett.* **1999**, *1*, 2165−2167.
(89) Rathman, T. L.; Schwindeman, J. A. Preparation, Properties, and Safe Handling of Commercial Organolithiums: Alkyllithiums, Lithium sec-Organoamides, and Lithium Alkoxides. *Org. Proc. Res. Dev.* **2014**, *18*, 1192−1210.
(90) Schlosser, M.; Spahić, B.; Van Chau, L. Stereoselektivität diastereogener CC-Verknüpfungen II Eine Carben/Carbenoid-Kaskade und ≪Hypermechanismen≫. *Helv. Chim. Acta* **1975**, *58*, 2586−2594.
(91) Lishchynskyi, A.; Miloserdov, F. M.; Martin, E.; Benet-Buchholz, J.; Escudero-Adán, E. C.; Konovalov, A. I.; Grushin, V. V. The Trifluoromethyl Anion. *Angew. Chem., Int. Ed.* **2015**, *54*, 15289−15293.
(92) Uneyama, K.; Katagiri, T.; Amii, H. α-Trifluoromethylated Carbanion Synthons. *Acc. Chem. Res.* **2008**, *41*, 817−829.
(93) Schlosser, M.; Heinz, G.; Chau, L. V. Fluororganische Synthesen, II. Fluorchlorcyclopropane - ihre Darstellung und Abwandlung. *Chem. Ber.* **1971**, *104*, 1921−1933.
(94) Novikov, M. A.; Ibatov, Y. A.; Volchkov, N. V.; Lipkind, M. B.; Semenov, S. E.; Nefedov, O. M. Copper-catalyzed ligand free ring-opening amination of gem-fluorohalocyclopropanes − An efficient route toward 2-fluoroallylamines. *J. Fluor. Chem.* **2017**, *194*, 58−72.
(95) Bychek, R.; Mykhailiuk, P. K. A Practical and Scalable Approach to Fluoro-Substituted Bicyclo[1.1.1]pentanes. *Angew. Chem., Int. Ed.* **2022**, *61*, No. e202205103.
(96) Fang, Z.; Cordes, D. B.; Slawin, A. M. Z.; O'Hagan, D. Fluorine containing cyclopropanes: synthesis of aryl substituted all-cis 1,2,3-trifluorocyclopropanes, a facially polar motif. *Chem. Commun.* **2019**, *55*, 10539−10542.
(97) V Dehmlow, E.; Broda, W. Anwendungen der Phasentransfer-Katalyse, 23. Notiz über Bromiodcarben und zugehörige Halogen-austausch-prozesse. *Chem. Ber.* **1982**, *115*, 3894−3897.
(98) Mathias, R.; Weyerstahl, P. Stabile 1,1-Dijod-und 1-Chlor-1-jod-cyclopropane. *Angew. Chem.* **1974**, *86*, 42−43.
(99) Pace, V.; Monticelli, S.; de la Vega-Hernandez, K.; Castoldi, L. Isocyanates and isothiocyanates as versatile platforms for accessing (thio)amide-type compounds. *Org. Biomol. Chem.* **2016**, *14*, 7848−7854.
(100) Pace, V.; Castoldi, L.; Holzer, W. Addition of lithium carbenoids to isocyanates: a direct access to synthetically useful N-substituted 2-haloacetamides. *Chem. Commun.* **2013**, *49*, 8383−8385.
(101) Kaljurand, I.; Kütt, A.; Sooväli, L.; Rodima, T.; Mäemets, V.; Leito, I.; Koppel, I. A. Extension of the Self-Consistent Spectrophotometric Basicity Scale in Acetonitrile to a Full Span of 28 pKa Units: Unification of Different Basicity Scales. *J. Org. Chem.* **2005**, *70*, 1019−1028.
(102) Pace, V.; Castoldi, L.; Mamuye, A. D.; Holzer, W. Homologation of Isocyanates with Lithium Carbenoids: A Straightforward Access to α-Halomethyl- and α,α-Dihalomethylamides. *Synthesis* **2014**, *46*, 2897−2909.
(103) Touqeer, S.; Senatore, R.; Malik, M.; Urban, E.; Pace, V. Modular and Chemoselective Strategy for Accessing (Distinct) α,α-Dihaloketones from Weinreb Amides and Dihalomethyllithiums. *Adv. Synth. Catal.* **2020**, *362*, 5056−5061.
(104) Bull, J. A.; Charette, A. B. Improved Procedure for the Synthesis of gem-Diiodoalkanes by the Alkylation of Diiodomethane. Scope and Limitations. *J. Org. Chem.* **2008**, *73*, 8097−8100.
(105) Bull, J. A.; Mousseau, J. J.; Charette, A. B. Convenient One-Pot Synthesis of (E)-β-Aryl Vinyl Halides from Benzyl Bromides and Dihalomethanes. *Org. Lett.* **2008**, *10*, 5485−5488.
(106) Krasovskiy, A.; Krasovskaya, V.; Knochel, P. Mixed Mg/Li Amides of the Type R2NMgCl·LiCl as Highly Efficient Bases for the Regioselective Generation of Functionalized Aryl and Heteroaryl Magnesium Compounds. *Angew. Chem., Int. Ed.* **2006**, *45*, 2958−2961.
(107) Monticelli, S.; Urban, E.; Langer, T.; Holzer, W.; Pace, V. A Straightforward Homologation of Carbon Dioxide with Magnesium Carbenoids en Route to α-Halocarboxylic Acids. *Adv. Synth. Catal.* **2019**, *361*, 1001−1006.
(108) Senatore, R.; Malik, M.; Pace, V. Fluoroiodomethane: A CH2F-Moiety-Delivering Agent Suitable for Nucleophilic-, Electrophilic-, and Radical-Harnessed Operations. *Adv. Synth. Catal.* **2022**, *364*, 2890−2910.
(109) Monticelli, S.; Colella, M.; Pillari, V.; Tota, A.; Langer, T.; Holzer, W.; Degennaro, L.; Luisi, R.; Pace, V. Modular and Chemoselective Strategy for the Direct Access to α-Fluoroepoxides and Aziridines via the Addition of Fluoroiodomethyllithium to Carbonyl-Like Compounds. *Org. Lett.* **2019**, *21*, 584−588.
(110) Colella, M.; Tota, A.; Großjohann, A.; Carlucci, C.; Aramini, A.; Sheikh, N. S.; Degennaro, L.; Luisi, R. Straightforward chemo- and stereoselective fluorocyclopropanation of allylic alcohols: exploiting the electrophilic nature of the not so elusive fluoroiodomethyllithium. *Chem. Commun.* **2019**, *55*, 8430−8433.
(111) Fasano, V.; Winter, N.; Noble, A.; Aggarwal, V. K. Divergent, Stereospecific Mono- and Difluoromethylation of Boronic Esters. *Angew. Chem., Int. Ed.* **2020**, *59*, 8502−8506.

https://doi.org/10.1021/acs.jpca.5c08066
J. Phys. Chem. A 2026, 130, 1790−1803